Conjugate Gradient Method in Hilbert and Banach Spaces to Enhance the Spatial Resolution of Radiometer Data

Flavia Lenti, *Student Member, IEEE*, Ferdinando Nunziata, *Senior Member, IEEE*, Claudio Estatico, and Maurizio Migliaccio, *Senior Member, IEEE*

***Abstract*—In this paper, a new computer-time effective iterative method is proposed to enhance the spatial resolution of microwave radiometer data in both Hilbert and Banach spaces. The reconstruction method is based on the conjugate gradient (CG) method. CG is a well-known method in electromagnetics, where it is commonly used to address inverse problems in Hilbert spaces. However, the method has never been applied to inverse problems related to spatial resolution enhancement of microwave remotely sensed measurements. In this paper, CG is adapted to the microwave radiometer case and exploited to reconstruct the brightness field at enhanced spatial resolution. Then, CG is, for the first time, extended to Banach spaces by means of duality maps and then applied to enhance the radiometer spatial resolution. Experiments undertaken on both simulated and actual radiometer data confirm the soundness of the proposed approach in Banach spaces and demonstrate that CG is able to provide a reconstruction accuracy similar to the conventional Landweber method, but with a significantly reduced processing time.**

***Index Terms*—Inverse problems, microwave radiometry, resolution enhancement.**

I. Introduction

SATELLITE remote sensing is the fundamental tool for Earth observation applications. Satellites enable a global view of the Earth. Clouds, forests, land, ocean, ice, etc., can be observed in a very effective way from the space. Remote sensing provides typically indirect measurements, i.e., the unknown function needs to be estimated from remotely sensed measurements. Hence, an inverse problem has to be solved, which can be generally formulated according to a Fredholm integral equation of the first kind, i.e.,

$$b_t = \int_{\Omega} G_t(z) f(z) dz \tag{1}$$

where b_t is the tth measurement, with $t = 1, \ldots, m$, $f(\cdot)$ is the unknown function to be retrieved, and $G_t(\cdot)$ is the low-pass system aperture function. Equation (1) is an ill-posed linear problem that, when the kernel $G_t(\cdot)$ is band limited, can be discretized as [1]

$$\mathbf{A}_t^T \mathbf{x} = b_t \tag{2}$$

where $\mathbf{A}_t \in \mathbf{R}^n$ is the sampling of $G_t(\cdot)$, and $\mathbf{x} \in \mathbf{R}^n$ is the equispaced sampled version of the continuous signal $f(\cdot)$. To estimate a band-limited version of f from m measurements, $\mathbf{b} = (b_1, b_2, \ldots, b_m)$, the following linear system is to be solved:

$$A\mathbf{x} = \mathbf{b} \tag{3}$$

where $A = (\mathbf{A}_1, \mathbf{A}_2, \ldots, \mathbf{A}_m)^T$. The problem may be fully determined, overdetermined, or underdetermined. In most remote sensing applications, A is underdetermined. This is the case of spatial resolution enhancement methods that, once a low-resolution measurement of the geophysical parameters is provided, attempt to reconstruct them on a finer resolution grid, exploiting the partial correlation of the measurements [2]. Spatial resolution enhancement methods are typically applied to microwave scatterometer and radiometer remotely sensed data. The latter call for a dense spatial/temporal coverage, but they are characterized by a spatial resolution that, although satisfactory for mesoscale applications, is not enough for regional-scale purposes. In this paper, reference is made to the microwave radiometer.

To enhance the spatial resolution of radiometer data, the linear problem (1), which can be considered as the analog of the antenna pattern deconvolution, is to be solved. In this case, $G_t(\cdot)$ is a smooth function related to the projected antenna patterns, $f(\cdot)$ is the brightness field T_B, and b_t is the tth antenna temperature (T_{A_t}) [2]. The unknown brightness field T_B and the measurements T_A are represented by $n_1 \times n_2$ and $m_1 \times m_2$ matrices, with $n_1 > m_1$ and $n_2 > m_2$. Hence, to retrieve T_B on a finer spatial resolution grid, a linear underdetermined system

Manuscript received April 14, 2015; revised July 14, 2015; accepted July 15, 2015.

F. Lenti is with Université de Toulouse, INP, IRIT et Centre Europen de Recherche et de Formation Avance en Calcul Scientifique (CERFACS), Toulouse 31000, France (e-mail: flavia.lenti@irit.fr).

F. Nunziata is with the Dipartimento di Ingegneria, Università degli Studi di Napoli "Parthenope," 80143 Napoli, Italy, and also with Shanghai Ocean University, Shanghai 200090, China (e-mail: ferdinando.nunziata@uniparthenope.it).

C. Estatico is with the Dipartimento di Matematica, Università degli Studi di Genova, 16132 Genova, Italy (e-mail: estatico@dima.unige.it).

M. Migliaccio is with the Dipartimento di Ingegneria, Università degli Studi di Napoli "Parthenope," 80143 Napoli, Italy, and also with Nova Southeastern University, Fort Lauderdale, FL 33314 USA (e-mail: maurizio.migliaccio@uniparthenope.it).

Color versions of one or more of the figures in this paper are available online at http://ieeexplore.ieee.org.

Digital Object Identifier 10.1109/TGRS.2015.2458014

has to be solved. The system has infinite solutions and is ill conditioned; hence, constraints must be imposed on the sought solution. In the frame of spatial resolution enhancement of microwave data, different choices are suitable [2]–[8]. Among the possible constraints, the minimum p-norm, with $1 < p \leq 2$, results in reconstructions spanning from Hilbert $(p = 2)$ to Banach $(1 < p < 2)$ spaces.

When $p = 2$, the well-known 2-norm is achieved. In the literature, many algorithms have been proposed to enhance the spatial resolution of microwave radiometer data, based on the minimum 2-norm constraint. These methods can be divided into two main categories: direct and iterative. Direct methods, e.g., truncated singular value decomposition [3], [9], Tikhonov [10], and Backus–Gilbert [6], [7], are based on standard decompositions in numerical linear algebra. Iterative methods, e.g., Landweber method [4] and algebraic reconstruction technique [11], [12], rely on an iterative scheme that converges to the desired solution. Many iterative schemes can be considered as regularization methods, where the iteration number plays the role of regularization parameter. Usually, the choice of the 2-norm gives rise to smooth (sometimes oversmooth) solutions and Gibbs-related oscillations, where abrupt discontinuities are present. This is a key problem, for instance, on the boundary between land and ocean for radiometer measurements. In fact, the actual raw measurements blur the land/ocean boundary, giving rise to biased measurements along the coast. This blurring effect is even more noticeable when small islands are present. Due to their small size, the measurements are smeared not only along the coastline but also throughout the interiors [7]. Recently, to overcome the drawbacks related to the 2-norm, the resolution enhancement problem has been cast in the Banach spaces [4]. Unlike the L^2 space, the L^p space, for $p \neq 2$, is not a Hilbert space, but is only a Banach space [13]. A Banach space is a complete normed linear space, which is not equipped with any scalar product. This means that, despite of Hilbert spaces where the scalar product is defined, in Banach spaces, the "angle" between two elements is not defined, and hence, it has no meaning.

No direct method can be applied in Banach spaces due to the intrinsic nonlinearity of the inverse operator [13]. With respect to iterative methods, only the Landweber method has been extended to the Banach spaces and applied to enhance the spatial resolution of both simulated and actual microwave radiometer data [4]. Results show that, due to the geometrical properties of Banach spaces, the regularization method allows obtaining solutions endowed with lower oversmoothness and reduced Gibbs oscillations. However, the key drawback of the Landweber method is its very slow convergence rate. To overcome this drawback, in this study, a new iterative scheme in Banach spaces is proposed that is an extension of the conventional conjugate gradient (CG) method in Hilbert spaces.

CG belongs to the class of conjugate direction (CD) methods that are well known for their computer-time effectiveness and stability in solving a set of linear equations. CG is the most famous CD method, and it is such that the solution provided at the kth step is a combination of the solution at the previous step and descent direction vector.

CG is a iterative method that has been widely employed to solve operator equations arising in electromagnetics [14]. In [14]–[16], the basic principles of CD methods are developed, and CG is derived as a special case. It is shown that it exhibits the advantages of both a direct method, as it converges to the solution in a finite number of steps, and that of an iterative method, as it provides a stable computational process that allows dealing with ill-conditioned problems. CG has been applied to scattering problems related to thin-wire antennas and conducting dielectric cylinders [17], [18], whereas in [19], CG is applied to evaluate the solution of magnetic field integral equation for 2-D perfectly conducting rough surfaces. In [20], tomographic imaging of isolated ground surfaces is addressed using ground wave propagation, whereas the inverse problem is solved using CG. To the best of our knowledge, CG has never been applied to inverse problems arising in microwave remote sensing. Moreover, the aforementioned applications always refer to CG in Hilbert spaces.

In this paper, CG is first applied to enhance the spatial resolution of microwave radiometer measurements. The inversion problem is addressed in Hilbert spaces, adapting the conventional CG computational scheme to the microwave radiometer case. Then, CG is extended to the more involving Banach spaces to solve the inversion problem in such spaces and, hence, to better retrieve abrupt discontinuities. Numerical experiments are undertaken on both simulated and actual radiometer data collected by Special Sensor Microwave/Imager (SSM/I) and Advanced Microwave Scanning Radiometer for EOS (AMSR-E) radiometers. Reconstructions obtained using CG are contrasted with the ones obtained using the conventional Landweber method in both Hilbert and Banach spaces. Results demonstrate the soundness of the proposed approach in both spaces. CG is able to provide the same reconstruction accuracy of the Landweber method, but with a significant reduction of the processing time. Hence, the proposed approach makes spatial resolution enhancement of microwave radiometer data feasible for real-time applications even in Banach spaces.

This paper is organized as follows. In Section II, the inversion procedure is described in both Hilbert and Banach spaces. Numerical experiments undertaken on both simulated and actual data are described in Section III. The conclusions are drawn in Section IV.

II. Theory

Here, the theoretical aspects of the inversion procedure proposed to enhance the spatial resolution of the coarse but partially correlated 2-D radiometer measurements are described.

The approach to find the solution of the discretized problem (3) can be formulated in a generic $l^p(\mathbf{R}^n)$ space as the minimization of the p-norm of the residual

$$\Omega_p(\mathbf{x}) = \frac{1}{p}\|A\mathbf{x} - \mathbf{b}\|_p^p \tag{4}$$

where $l^p(\mathbf{R}^n) = \{\mathbf{x} : \sum_{k=1}^{n} |x_k|^p < \infty, x_i \in \mathbf{R}\}$ (hereinafter l^p), $\|\mathbf{x}\|_p^p = \sum_{i=1}^{n} |x_i|^p$, and the subscript i means that the ith component of the vector is considered.

The p-norm is the discrete version of the norm of the space L^p, which is the space of the p-power integrable functions on

the 2-D domain. We note that, if $p = 2$, $\Omega_2(\mathbf{x})$ is the classical 2-norm of the residual. The class of iterative methods to minimize $\Omega_p(\mathbf{x})$ is the gradient-like one, whose $(k+1)$th iteration is given by

$$\mathbf{x}_{k+1} = \mathbf{x}_k + \alpha_k \mathbf{p}_k \tag{5}$$

where $\mathbf{x}_0$ is an arbitrary initial guess, $\alpha_k > 0$ is the so-called step size, and $\mathbf{p}_k$ is a descent direction at point $\mathbf{x}_k$ for Ω_p, i.e., $\mathbf{p}_k$ is a vector such that

$$\nabla\Omega_p(\mathbf{x}_k)^T \mathbf{p}_k \leq 0 \tag{6}$$

where $\nabla f(\mathbf{x}) \in \mathbf{R}^n$ denotes the gradient vector of the function $f(\mathbf{x}) \in \mathcal{R}^n$.

The classical approach is to choose $\mathbf{p}_k = -\nabla\Omega_p(\mathbf{x}_k)$, i.e., the one at the basis of the Landweber and steepest descent method [21]. The key drawback of this choice is the very slow convergence rate, particularly when dealing with ill-posed problems.

In this paper, a different approach is proposed based on the CG method. We recall that, in Hilbert spaces, CG allows a convergence rate significantly faster than the Landweber or steepest descent ones. In the following, CG is first reviewed in Hilbert spaces and then extended to the Banach ones.

A. CG in Hilbert Spaces

To describe CG in Hilbert spaces, it is worth recalling the generic iteration of gradient-like methods (5). The direction $\mathbf{p}_k$, according to (6), is a descent direction at point $\mathbf{x}_k$ for Ω_2. Different choices are possible for α_k and $\mathbf{p}_k$.

When the following choice is made

$$\begin{cases} \alpha_k & = \alpha \in \left(0, \frac{2}{\|A\|_2^2}\right] \\ \mathbf{p}_k & = -\nabla\Omega_2(\mathbf{x}_k) \end{cases} \tag{7}$$

the Landweber method is achieved [11].

The steepest descent method is obtained when the following choice is made:

$$\begin{cases} \alpha_k & = \min_\alpha \|A(\mathbf{x}_k + \alpha\mathbf{p}_k) - \mathbf{b}\|_2^2 \\ \mathbf{p}_k & = -\nabla\Omega_2(\mathbf{x}_k). \end{cases} \tag{8}$$

This choice of α_k allows for the fastest local convergence rate for the descent direction $\mathbf{p}_k$, and an explicit formula for its computation is available. However, both methods are still slow. To significantly improve the convergence rate, a different choice of $\mathbf{p}_k$ is possible, which lies at the basis of CG. In this case, α_k is generated again by the explicit formula for the minimization problem in (8), while a different descent direction is considered, namely, a linear combination of the current gradient and the previous direction, i.e.,

$$\mathbf{p}_k = -\nabla\Omega_2(\mathbf{x}_k) + \beta_k \mathbf{p}_{k-1} \tag{9}$$

where $\mathbf{p}_0 = -\nabla\Omega_2(\mathbf{x}_0)$.

Note that the choice of α_k (8) ensures that an arbitrary direction $\mathbf{p}_k$ is always a descent direction and that $\mathbf{x}_{k+1}$ is optimal with respect to the direction $\mathbf{p}_k$, i.e., $\nabla\Omega_2(\mathbf{x}_{k+1})^T\mathbf{p}_k = 0$. β_k is chosen to let $\mathbf{x}_{k+1}$ be optimal with respect to the direction $\mathbf{p}_{k-1}$, i.e.,

$$\beta_k : \nabla\Omega_2(\mathbf{x}_{k+1})^T \mathbf{p}_{k-1} = 0. \tag{10}$$

It can be proven that the choice of α_k and β_k ensures that $\mathbf{x}_k$ is optimal with respect to all the directions $\mathbf{p}_j$, with $j = 0, \ldots, k-1$. By using (8) and (10), it is easy to show that [21]

$$\begin{cases} \alpha_k = \frac{-A^*(A\mathbf{x}_k - \mathbf{b})^T \mathbf{p}_k}{(A^*A\mathbf{p}_k)^T \mathbf{p}_k}, \\ \beta_k = \frac{A^*(A\mathbf{x}_{k+1} - \mathbf{b})}{A^*(A\mathbf{x}_k - \mathbf{b})}. \end{cases} \tag{11}$$

where A^* is the adjoint operator of A. This allows achieving the exact solution of an $n \times n$ linear system of equation in at most n steps [21].

B. CG in Banach Spaces

Here, the CG method is extended to Banach spaces. The extension is not straightforward since, in Banach spaces, (9) is not well defined. To clarify this point, it is worth defining dual space and duality maps.

Let $\mathcal{X}$ be a Banach space; its dual space $\mathcal{X}^*$ is the space of all bounded linear functionals $x^* : \mathcal{X} \to \mathbf{R}$ equipped with the norm

$$\|x^*\|_{\mathcal{X}^*} = \sup_{\|x\|_{\mathcal{X}}=1} |x^*(x)|. \tag{12}$$

We recall that the dual space of l^p with $p > 1$ is l^q, with q being the Holder conjugate of p, i.e., $p^{-1} + q^{-1} = 1$ [22].

The duality map is a function that associates an element of the Banach space to an element of its dual [23]. In l^p spaces, the duality map $j_p : l^p \to l^q$ is a single-valued function that can be defined as [13]

$$j_p(\mathbf{x})_i = |x_i|^{p-1}\text{sign}(x_i) \tag{13}$$

where $i = 1, \ldots, n$, and the function $\text{sign} : \mathbf{R} \to \mathbf{R}$ is defined as

$$\text{sign}(x) = \begin{cases} 1, & \text{if} \quad x > 0, \\ 0, & \text{if} \quad x = 0, \\ -1, & \text{if} \quad x < 0. \end{cases} \tag{14}$$

We denote by $\mathbf{x}^*$ the element of l^q such that $j_p(\mathbf{x}) = \mathbf{x}^*$.

Once the dual space and duality map are defined, (9) can be analyzed in Banach spaces. It can be easily noted that, when $\nabla\Omega_2(\mathbf{x}_k)$ is replaced with $\nabla\Omega_p(\mathbf{x}_k)$, (9) is not well defined. To make it clear, we consider the first iteration

$$\begin{cases} \mathbf{x}_1 = \mathbf{x}_0 + \alpha_0\mathbf{p}_0, \\ \mathbf{p}_0 = -\nabla\Omega_p(\mathbf{x}_0) = -A^*\left[|A\mathbf{x} - \mathbf{b}|^{p-1} \circ \text{sign}(A\mathbf{x} - \mathbf{b})\right] \\ \qquad\qquad = -A^* j_p(A\mathbf{x}_0 - \mathbf{b}) \end{cases} \tag{15}$$

where $\circ$ is the componentwise product. We recall that $A^* : l^q \to l^q$ is the adjoint of the operator $A : l^p \to l^p$, i.e.,

$$\langle Ax, y\rangle = \langle x, A^*y\rangle \quad \forall\, x \in l^p \text{ and } y \in l^q \tag{16}$$

where $< x, y > = < y, x > = y(x)$. We note that, since $\mathbf{p}_0 \in l^q$ (hereinafter $\mathbf{p}_0^*$) and $\mathbf{x}_0 \in l^p$, the sum in (15) is not well defined. To overcome this problem, the duality map $j_p : l^q \to l^p$ must be invoked to define the iteration as $\mathbf{x}_1^* = j_p(\mathbf{x}_0) + \alpha_0 \mathbf{p}_0^*$. In order to obtain the sought solution in l^p, the $j_q(\cdot)$ duality map must be applied, i.e.,

$$\mathbf{x}_1 = j_q\left(\mathbf{x}_1^*\right). \tag{17}$$

The duality map $j_q : l^q \to l^p$ is the inverse of $j_p(\cdot)$. As a matter of fact, the $(k+1)$th iteration is given by

$$\begin{cases} \mathbf{x}_{k+1} = j_q\left(j_p(\mathbf{x}_k) + \alpha_k \mathbf{p}_k^*\right), \\ \mathbf{p}_{k+1}^* = -\nabla \Omega_p(\mathbf{x}_k) + \beta_k \mathbf{p}_k^*. \end{cases} \tag{18}$$

The choice of α_k and β_k is based on the theoretical rationale developed in [24], where the CG has been demonstrated to strongly converge to the minimum p-norm solution of (3). Accordingly, α_k is given by

$$\alpha_k : \min_{\alpha \in [0, T_k]} \left\| A j_q\left(\mathbf{x}_k^* + \alpha \mathbf{p}_k^*\right) - \mathbf{b} \right\|_p^p \tag{19}$$

where

- $T_k = \min\{(R_k^p(V_k - d\|A\|_q Q_k)/G_q 2^{q-2}\|\mathbf{x}_k^*\|_q^{(q-2)}(q-1)\|A\|^2 R_k^{2(p-1)} Q_k^2), (\|\mathbf{x}_k^*\|_q / \|A\| R_k^{p-1} Q_k)\}$.
- $R_k = \|A\mathbf{x}_k - \mathbf{b}\|_p$.
- $Q_k = (1 - \gamma^{k+1})/(1-\gamma)$.
- $V_k = 1 - ((2^p - 1)/p)((\gamma - \gamma^{k+1})/(1-\gamma))$.
- $d \le (1 - ((2^p - 1 + p)/p)\gamma)(1/\|A\|)$.
- G_q is a constant that depends on l^q [23].

It must be explicitly pointed out that the functional (19) is nonlinear. Following the rationale of CG in Hilbert spaces, β_k is given by the generalization of the Fletcher–Reeves formula [25], that is [24]

$$\beta_k = \gamma \frac{R_k^p}{R_{k-1}^p} \tag{20}$$

where $0 < \gamma < (p/(2^p - 1 + p))$ is a constant relaxation parameter. As a matter of fact, the $(k+1)$th iteration is given by (18). Note that, when $\gamma = 0$, the steepest descent method in Banach spaces is obtained. It must be pointed out that, unlike Hilbert spaces, when CG is applied in Banach spaces, it does not necessarily reach the solution of the problem (3) in at most n steps, although the convergence holds [26].

To understand the performance of reconstructions in Banach spaces in terms of oversmoothness and reduction of Gibbs oscillations, it is worth analyzing deeply the generic iteration (18), i.e.,

$$\mathbf{x}_{k+1} = j_q\left(\mathbf{x}_{k+1}^*\right). \tag{21}$$

According to (13), the behavior of $j_q(\cdot)$ depends on p. When $1 < p < 2$, i.e., $q > 2$, the ith component of the dual iteration $\mathbf{x}_{k+1}^*$ is transformed as follows:

$$\begin{cases} \left|j_q\left(\mathbf{x}_{k+1}^*\right)_i\right| < \left|\left(\mathbf{x}_{k+1}^*\right)_i\right|, & \text{if } \left|\left(\mathbf{x}_{k+1}^*\right)_i\right| < 1, \\ \left|j_q\left(\mathbf{x}_{k+1}^*\right)_i\right| > \left|\left(\mathbf{x}_{k+1}^*\right)_i\right|, & \text{if } \left|\left(\mathbf{x}_{k+1}^*\right)_i\right| > 1. \end{cases} \tag{22}$$

In simple terms, $j_q(\cdot)$ for $q > 2$ is such that the small components of $\mathbf{x}_{k+1}^*$ (i.e., $|(\mathbf{x}_{k+1}^*)_i| < 1$) are reduced, whereas the large components (i.e., $|(\mathbf{x}_{k+1}^*)_i| > 1$) are emphasized, allowing low ringing effects in the iteration $\mathbf{x}_{k+1}$. Following this theoretical rationale, the choice of p is here accomplished in order to provide the best tradeoff between reconstruction performance and algorithm's stability [4]. The value here adopted is $p = 1.2$.

It must be noted that, since the 1-D minimization problem (19) is nonlinear, tailored techniques must be applied. In this paper, the recent and efficient derivative-free method for bound-constrained optimization (BCDFO) is used [27], which is based on an iterative trust-region method.

A key point when dealing with iterative regularization techniques is the choice of the iteration number, which plays the role of regulation parameter. The discrepancy principle [11] is here specialized to the l^p space to stop the iterations in an objective and unsupervised way. It consists of choosing the smallest iteration number k such that

$$\|A\mathbf{x}_k - \mathbf{b}\|_p \le c\delta_e \tag{23}$$

where δ_e is an upper bound of the p-norm of the error, and $c \ge 1$ is a constant, which, in our study, is equal to 1.

III. Numerical Experiments

Here, numerical experiments are undertaken to discuss the reconstruction performance of CG in both Hilbert and Banach spaces with respect to the conventional Landweber method.

Both simulated and actual radiometer data are considered. The latter refer to SSM/I and AMSR-E radiometers. SSM/I is a total-power seven-channel four-frequencies radiometer, whose channels are given by 19.35-, 37.0-, and 85.5-GHz measurements accomplished at both vertical (V) and horizontal (H) polarization and 22.235-GHz V-polarized measurements (see Table I). The radiometer orbital altitude is 833 km, with a nominal swath width of about 1400 km. Along with the along-scan direction, it performs 128 measurements at the two 85.5-GHz channels and 64 measurements at the remaining five channels [28]. AMSR-E is a total-power 12-channel, six-frequency, and dual-polarization radiometer, whose channels are given by 6.9-, 10.7-, 18.7-, 23.8-, 36.5-, and 89.0-GHz V- and H-polarized measurements (see Table I). At an altitude of 705 km, it measures the upwelling scene brightness temperatures over an angular sector of $\pm 61^\circ$, resulting in a swath width of 1445 km. The AMSR-E measurements are recorded at equal intervals of 10 km (5 km for the 89-GHz channels) along the scan.

In all the subsequent experiments, the SSM/I and AMSR-E projection of the integrated antenna pattern on the surface is approximated by a Gaussian function. A 3-dB main lobe of about 69 × 43 km (75 km × 43 km) is considered for the 19-GHz SSM/I measurements (6.9-GHz AMSR-E measurements).

Numerical experiments on simulated data refer to the SSM/I configuration. A 1400 × 900 km reference brightness field, whose pixel is 13 pixel/deg, is generated. SSM/I measurements

TABLE I
MAIN CHARACTERISTICS OF THE SSM/I AND AMSR-E RADIOMETERS

SSM/I radiometer				
Channel		3 dB effective field of view on Earth Surface (km)		Spacing (km)
Frequency (GHz)	Pol.	Along-track	Cross-track	Along-track
19.35	V	69	43	25
19.35	H	69	43	25
22.235	V	50	40	25
37.0	V	37	28	25
37.0	H	37	28	25
85.5	H	15	13	12.5
85.5	V	15	13	12.5
AMSR/E radiometer				
Channel		3 dB effective field of view on Earth Surface (km)		Spacing (km)
Frequency (GHz)	Pol.	Along-track	Cross-track	Along-track
6.9	V	75	43	10
6.9	H	75	43	10
10.6	V	51	29	10
10.6	H	51	29	10
18.7	V	27	16	10
18.7	H	27	16	10
23.8	V	32	18	10
23.8	H	32	18	10
36.5	V	14	8	10
36.5	H	14	8	10
89.0	V	7	4	5
89.0	H	7	4	5

are obtained using (3), where the generic line of the matrix A is given discretizing [2], [3]

$$\exp\left\{-\log(2)\left[\left(\frac{\gamma-\gamma_1}{\gamma_0}\right)^2+\left(\frac{\vartheta-\vartheta_1}{\vartheta_0}\right)^2+\xi(\gamma-\gamma_1)(\vartheta-\vartheta_1)\right]\right\} \tag{24}$$

where γ_1 and ϑ_1 are the azimuth and elevation angles of the boresight pointing of the antenna, respectively; γ_0 and ϑ_0 are the corresponding 3-dB main lobe; and ξ allows a rotation of the aperture footprint and depends on the azimuth angle of the boresight pointing of the antenna.

To simulate noisy measurements, a zero-mean additive Gaussian noise is considered [8]. Moreover, to test the method in a challenging environment, a 5-K noise level is adopted.

The first experiment refers to the brightness reference field shown in Fig. 1(a). The field consists of

1) Equiamplitude and nonuniformly spaced lines, whose width and amplitude level are 40 samples and 100 K, respectively. In detail, seven lines are horizontally oriented [labeled "A1" to "A7" in Fig. 1(a)] and characterized by a spacing ranging from 10 up to 60 samples; eight lines are vertically oriented [labeled "B1" to "B8" in Fig. 1(a)] calling for a spacing ranging from 10 up to 70 samples.
2) Uniformly spaced (40 samples) hot spots calling for different amplitudes and dimensions: six vertically oriented hot spots [labeled "C1" to "C6" in Fig. 1(a)] whose size is 30×30 samples that call for an amplitude ranging from 10 K up to 110 K; six horizontally oriented hot spots [labeled "D1" to "D6" in Fig. 1(a)] whose size is 40×40 samples that call for an amplitude ranging from 10 to 110 K.
3) Uniformly spaced (40 samples) and equiamplitude (100 K) hot spots calling for different dimensions; six vertically oriented hot spots [labeled "E1" to "E6" in Fig. 1(a)] calling for dimension ranging from 10×20 to 60×70 samples, seven horizontally oriented hot spots (labeled "F1" to "F7") calling for dimensions ranging from 10×10 to 70×70 samples.

The simulated noisy measurements are shown in Fig. 1(b), where the SSM/I pixel spacing, i.e., 21.8×25 samples, applies. It can be noted that both the lines and the hot spots are not resolved.

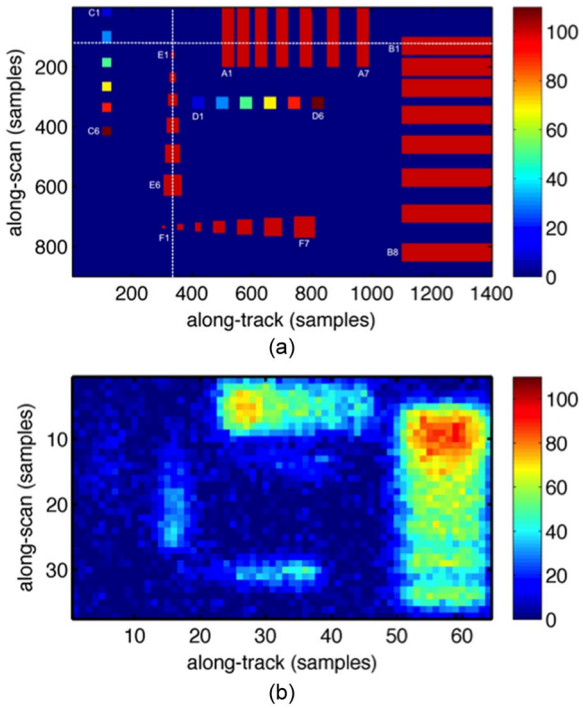

Fig. 1. (a) Reference brightness field related to an area of 1400 × 900 km, where some discontinuities of different sizes, amplitudes, and spacing are present. (b) Simulated noisy measurements obtained by considering SSM/I parameters and a 5-K additive noise level.

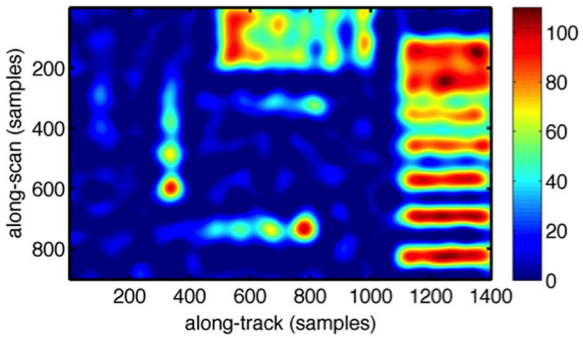

Fig. 2. Reconstructed field obtained by CG2.

The reconstructed field at enhanced spatial resolution obtained using CG in Hilbert space (CG2) is shown in Fig. 2. It can be noted that most lines and hot spots are correctly resolved and edges are adequately well defined.

Horizontally and vertically oriented lines [see "A" and "B" in Fig. 1(a)], which cannot be separated in the measurement field of Fig. 1(b), can be now recognized. In detail, horizontally oriented lines are retrieved better than the vertically oriented ones due to their larger size and the finer spatial resolution in the along-track direction. With respect to vertically and horizontally oriented equal-size hot spots [see "C" and "D" in Fig. 1(a)], which are badly visible in the measurement field of Fig. 1(b), only few hints related to the largest amplitude hot spots ("C5", "C6" and "D5", "D6") are clearly distinguishable. With respect to vertically and horizontally oriented equal-amplitude hot spots [see "E" and "F" in Fig. 1(a)], which are not resolved in the measurement field, only the largest ones

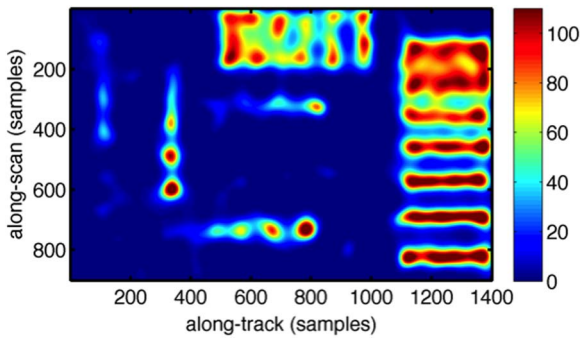

Fig. 3. Reconstructed field obtained by CG12.

("E4"- "E6" and "F4"-"F7") are correctly resolved. Note that, in all the cases, the amplitude level is generally underestimated, and Gibbs oscillations are clearly visible, which may be misunderstood as hot spots.

The reconstructed field at enhanced spatial resolution obtained using CG in $l^{1,2}$ (CG12) is shown in Fig. 3. It can be noted that the lines and hot spots distinguished in Hilbert spaces are distinguished also in $l^{1,2}$. However, edges are better defined, and Gibbs oscillations are significantly reduced. In addition, the amplitude level is generally better reconstructed, although in same cases ("B8", "E6," and "F7"), it is over-estimated.

In order to analyze in depth the reconstruction performance, an along-track transect is considered [see Fig. 1(a)], and the correspondent values of the reference field (black line) and the field reconstructed at enhanced resolution by using CG2 (red line) and CG12 (cyan line) are plotted in Fig. 4(a). Note that the reconstructions obtained by using the conventional Landweber method in l^2 and $l^{1,2}$ spaces (LW2 and LW12, respectively) are also shown for reference purposes. It can be noted that lines "A4"-"A7," and "B1" are well detected by both CG2 and CG12. Some signals related to the lines "A3" can be recognized in the CG12 reconstruction. Lines "A1" and "A2" cannot be separated by neither CG2 nor CG12. This implies that those equiamplitude horizontally oriented lines can be distinguished by the CG2 and CG12 methods once their separation is larger than 30 and 20 samples, respectively. In addition, CG2 significantly underestimates all the amplitudes, whereas better results are obtained using CG12 that, for instance, correctly estimates "A7." With respect to the hot spot "C2," well-distinguishable signals are present in the CG12 reconstruction, whereas in the CG2 reconstruction, "C2" is not well distinguishable from Gibbs oscillations.

Reconstructed values obtained by using CG2, CG12, LW2, and LW12 are plotted along with the along-scan transect [see Fig. 1(a)] and shown in Fig. 4(b), where the reference field is also shown. It can be noted that hot spots "E4" to "E6" are well distinguished by both CG2 and CG12. The latter one results in an amplitude level reconstruction better than CG2 in all the cases, except "E6," where CG12 significantly overestimates the amplitude level.

CG2 reconstruction exhibits Gibbs oscillations both at the left- and the right-hand sides of the image. The latter completely hampers the signal related to "F1" to "F2" hot spots [see red circle in Figs. 1(a) and 4(b)]. However, this signal can

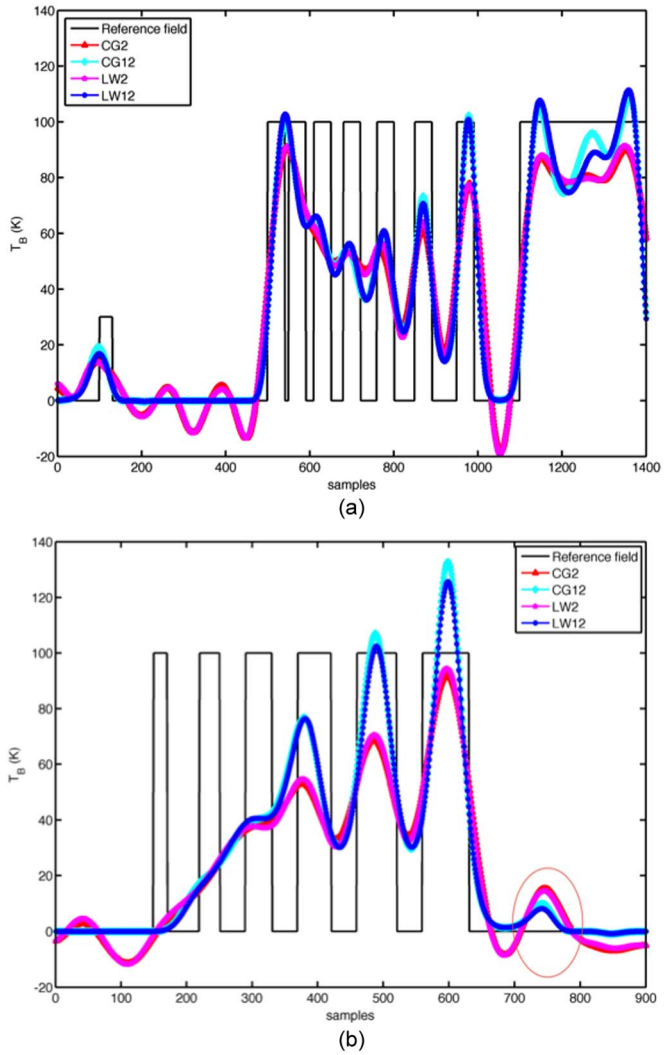

Fig. 4. (a) Along-track and (b) along-scan transects [see Fig. 1(a)] related to the (continuous black lines) reference field and the (triangle red line) CG2, (diamond cyan line) CG12, (pentagon magenta line) LW2, and (circle blue line) LW12 reconstructed fields at enhanced spatial resolution.

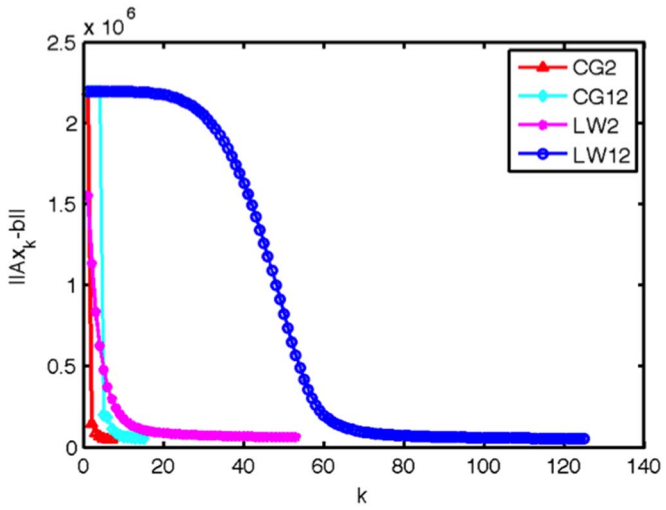

Fig. 5. 2-norm of the residual related to (triangle red line) CG2 and (pentagon magenta line) LW2. 1.2-norm of the residual related to (diamond cyan line) CG12 and (circle blue line) LW12 reconstructions.

TABLE II
PROCESSING TIME(S) OF CG2, CG12, LW2, AND LW12

Reference field	CG2 method	CG12 method	LW2 method	LW12 method
Fig.1(a)	2.4	28.3	16.4	165.8
Fig.6(a)	2.8	43.0	22.0	141.0
Fig.8(a)	85.3	750.2	337.1	3324.2

be well recognized in the CG12 reconstruction, which exhibits negligible Gibbs oscillations.

Plots in Fig. 4 confirm that CG reconstructions are similar to the conventional LW ones in both the Hilbert and Banach spaces. This can be further confirmed by analyzing the p-norm of the residual $\|A\mathbf{x}_k - \mathbf{b}\|_p^p$ versus the iteration number, as shown in Fig. 5, where the number of iterations needed to saturate the residuals is depicted for both CG and LW in l^2 and $l^{1.2}$. In the Hilbert spaces, the number of iterations to reach the solution by using CG is five times smaller that the LW one. In $l^{1.2}$, the iteration number is equal to 17 and 125 for CG and LW, respectively. It must be pointed out that the computational cost of each iteration is completely different for LW and CG. In the latter, a 1-D nonlinear functional (19) must be minimized at each iteration. However, when the BCDFO minimization procedure is adopted, CG12 is very effective, as one can note in Table II, where the processing times of CG2, CG12, LW2, and LW12 are listed. CG2 (CG12) results in a processing time about eight (six) times faster than LW2 (LW12).

The following experiments are undertaken on actual 19-GHz H-polarized SSM/I and 6.9-GHz V-polarized AMSR-E measurements.

The first experiment on actual data is relevant to the SSM/I data collected in 1998. The 1400 × 900 km brightness field that includes part of Italy, France, Spain, Algeria, and Tunisia is shown in Fig. 6(a) in false colors. This area is considered since it exhibits a large coastal zone that includes both abrupt discontinuities related to the land/sea interface and spotlike discontinuities related to small islands [see the Baleari archipelago on the left-hand side in Fig. 6(a)]. The low-pass nature of the microwave probe makes the edges very blurred and the coastline not well defined. The field reconstructed at enhanced spatial resolution by CG2 and CG12 is shown in Fig. 6(b) and (c), respectively. It can be noted that both outputs show better defined edges and coastlines. As expected, the reconstruction in $l^{1.2}$ space performs best in terms of reduction of oversmoothness and Gibbs oscillations. The abrupt discontinuities related to the land/sea interface are better defined, and both small islands belonging to the Baleari archipelago (Minorca and Ibiza) are much more visible. To analyze in depth the reconstruction performance, an along-scan transect is considered [see Fig. 6(a)], and the correspondent values of the nonenhanced brightness field (continuous black line) and the field reconstructed at enhanced spatial resolution using CG2 (dotted red line) and CG12 (dotted green line) are shown in Fig. 7. Note that reconstructions obtained using LW2 (crossed

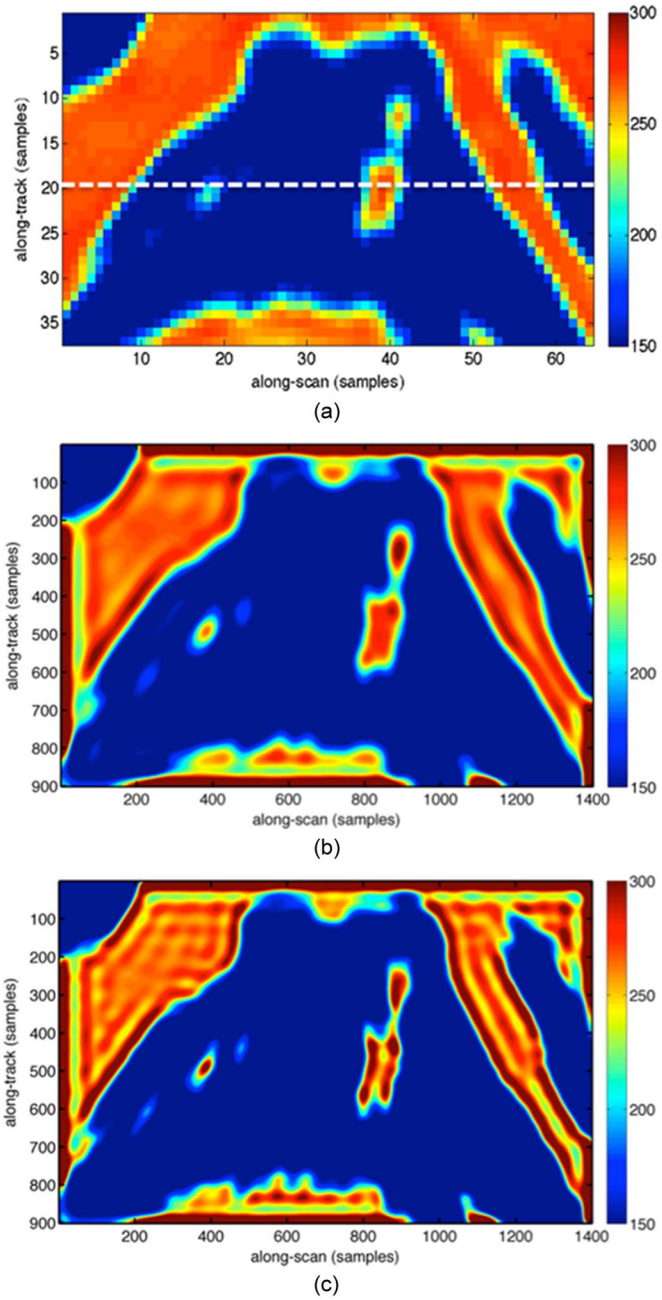

Fig. 6. (a) H-polarized brightness temperature field of 19 GHz. Brightness field reconstructed at enhanced spatial resolution using (b) CG2 and (c) CG12.

blue line) and LW12 (circle magenta line) are also shown for reference purposes. The isle of Majorca and the small Minorca island are more visible in all the reconstructions. Moreover, reconstructions in Banach space exhibit negligible Gibbs oscillations and result in a significant reduction of oversmoothness, leading to a better reconstruction of abrupt discontinuities. It can be noted that Banach reconstructions exhibit pronounced oscillations over the land area. This behavior has been theoretically addressed in [29], and it is actually due to the background that plays a key role when reconstructing in Banach spaces. In fact, in the $l^{1.2}$ space, a lower penalty term $\|\mathbf{x}\|_p$ is associated to elements with large but few components, and higher penalty is associated to many but small components

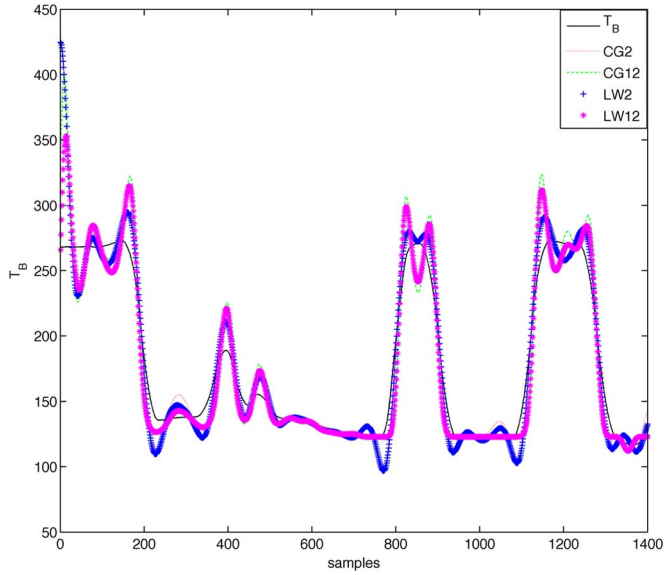

Fig. 7. Along-scan transect [see Fig. 6(a)] related to the (continuous black line) nonenhanced field, the (dotted red line) field reconstructed using CG2, (dotted green line) CG12, (crossed blue line) LW2, and (circle magenta line) LW12.

[29]. This implies that to let reconstruction methods working well in $l^{1.2}$, the background level is to be subtracted. In this paper, we focused on the sea/land interface; hence, we consider sea as reference. This justifies the smallest (largest) oscillations over sea surface (land). Note that CG and LW methods provide similar results in both spaces, while resulting in a completely different processing time as listed in Table II. CG2 (CG12) results in a processing time about seven (three) times faster than LW2 (LW12).

The second experiment on actual data is relevant to the AMSR-E data collected on March 21, 2007. The 956×7941 brightness field that is partially overlapped with the SSM/I one is shown in false colors in Fig. 8(a). Even in this case, although the AMSR-E spatial resolution is better than that of SSM/I (see Table I), edges are blurred, and the small islands that surround Majorca are barely visible. The field reconstructed at enhanced spatial resolution by CG2 and CG12 is shown in Fig. 8(b) and (c), respectively. Results agree with the one obtained processing SSM/I measurements. Hence, edges are better defined in both spaces, and CG12 outperforms CG2 in terms of reconstruction quality, resulting in limited Gibbs oscillations and a significant reduction of oversmoothness. To quantitatively confirm this behavior, an along-scan transect is considered [see Fig. 8(a)], and the correspondent values of the nonenhanced brightness field (continuous black line) and the field reconstructed at enhanced spatial resolution using CG2 (dotted red line) and CG12 (dotted green line) are shown in Fig. 9, where reconstructions obtained using LW2 (cross blue line) and LW12 (circle magenta line) are also shown for reference purposes. Even in this case, one can note that Gibbs oscillations, which strongly affect Hilbert space reconstructions, are negligible in Banach reconstructions. Both islands are very well defined, and both the LW and CG methods provide similar results in both spaces, while resulting in a completely different processing times as listed in Table II. CG2 (CG12)

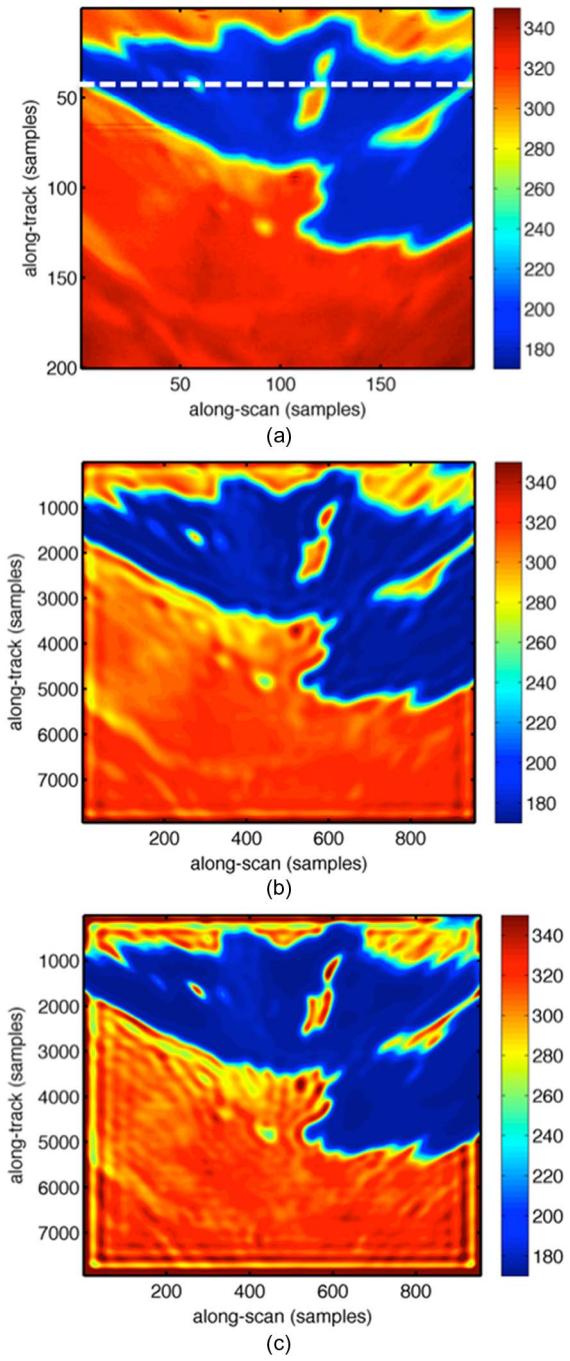

Fig. 8. (a) V-polarized brightness temperature field of 6.9 GHz. Brightness field reconstructed at enhanced spatial resolution using (b) CG2 and (c) CG12.

results in a processing time about six (four) times faster than LW2 (LW12).

IV. Conclusion

A new very computer-time effective iterative scheme has been proposed to enhance the spatial resolution of microwave radiometer data. The approach is based on CG that is here applied for the first time to inverse problems related to spatial resolution enhancement of microwave remotely sensed data. Spatial resolution enhancement is first addressed using CG in Hilbert spaces, and then, the method is extended, for the first time, to Banach spaces.

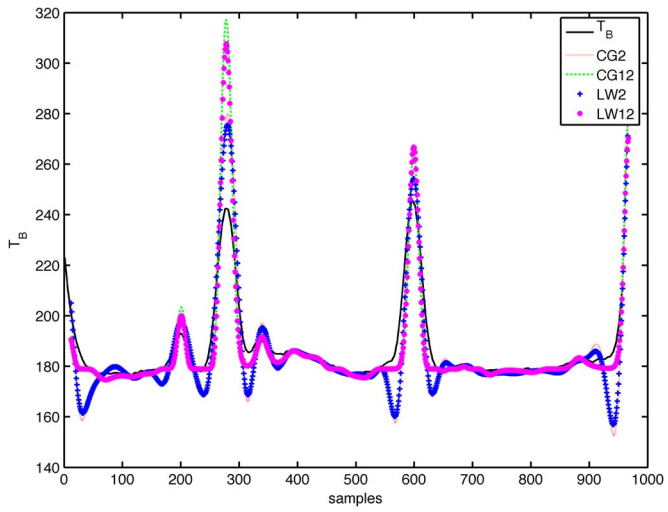

Fig. 9. Along-scan transect [see Fig. 8(a)] related to the (continuous black line) nonenhanced field and the field reconstructed using (dotted red line) CG2, (dotted green line) CG12, (crossed blue line) LW2, and (circle magenta line) LW12.

Experimental results, obtained using both simulated and actual radiometer data, confirm the soundness of the proposed approach. In addition, CG is also contrasted with the conventional Landweber method, and it is shown to achieve the same reconstruction accuracy, but with a significantly reduced processing time.

References

[1] B. Williams and D. Long, "Reconstruction from aperture-filtered samples with application to scatterometer image reconstruction," *IEEE Trans. Geosci. Remote Sens.*, vol. 49, no. 5, pp. 1663–1676, May 2011.

[2] D. Long, *Reconstruction and Resolution Enhancement Techniques for Microwave Sensors*. Singapore: World Scientific, 2003.

[3] F. Lenti, F. Nunziata, M. Migliaccio, and G. Rodriguez, "Two-dimensional TSVD to enhance the spatial resolution of radiometer data," *IEEE Trans. Geosci. Remote Sens.*, vol. 52, no. 5, pp. 2450–2458, May 2014.

[4] F. Lenti, F. Nunziata, C. Estatico, and M. Migliaccio, "On the spatial resolution enhancement of microwave radiometer data in Banach spaces," *IEEE Trans. Geosci. Remote Sens.*, vol. 52, no. 3, pp. 1834–1842, Mar. 2014.

[5] F. Lenti, F. Nunziata, C. Estatico, and M. Migliaccio, "Spatial resolution enhancement of Earth observation products using an acceleration technique for iterative methods," *IEEE Geosci. Remote Sens. Lett.*, vol. 12, no. 2, pp. 269–273, Feb. 2015.

[6] G. Backus and J. Gilbert, "Numerical applications of a formalism for geophysical inverse problem," *Geophys. J. Int.*, vol. 13, no. 1–3, pp. 247–276, Jul. 1967.

[7] M. Farrar and E. Smith, "Spatial resolution enhancement of terrestrial features using deconvolved SSM/I microwave brightness temperatures," *IEEE Trans. Geosci. Remote Sens.*, vol. 30, no. 2, pp. 349–355, Mar. 1992.

[8] D. Long and D. Daum, "Spatial resolution enhancement of SSM/I data," *IEEE Trans. Geosci. Remote Sens.*, vol. 36, no. 2, pp. 407–417, Mar. 1998.

[9] M. Migliaccio and A. Gambardella, "Microwave radiometer spatial resolution enhancement," *IEEE Trans. Geosci. Remote Sens.*, vol. 3, no. 5, pp. 1159–1169, May 2005.

[10] A. Gambardella and M. Migliaccio, "On the super resolution of microwave scanning radiometer measurements," *IEEE Geosci. Remote Sens. Lett.*, vol. 5, no. 4, pp. 796–800, Oct. 2008.

[11] P. Hansen, *Rank-Deficient and Discrete Ill-Posed Problem: Numerical Aspects of Linear Inversion*, vol. 4, ser. Monographs on Mathematica modeling and computation. Philadelphia, PA, USA: SIAM, 1998.

[12] H. Barrett and K. Myers, *Foundations of Image Science*. Hoboken, NJ, USA: Wiley-Interscience, 2004.
[13] T. Schuster, B. Kaltenbacher, B. Hofmann, and K. S. Kazimierski, *Regularization methods in Banach spaces*. ser. Radon Series on Computational and Applied Mathematics. New York, NY, USA: de Gruyter, 2012.
[14] T. Sarkar and E. Arvas, "On a class of finite step iterative methods (conjugate directions) for the solution of an operator equation arising in electromagnetics," *IEEE Trans. Antennas Propag.*, vol. 33, no. 10, pp. 1058–1066, Oct. 1985.
[15] T. Sarkar, "The conjugate gradient method as applied to electromagnetic field problems," *IEEE Antennas Propag. Newslett.*, vol. 28, no. 4, pp. 5–14, Aug. 1986.
[16] M. S. Frank and C. Balanis, "A conjugate direction method for geophysical inversion problems," *IEEE Trans. Geosci. Remote Sens.*, vol. GE-25, no. 6, pp. 691–701, Nov. 1987.
[17] H. H. Harada, D. J. N. Wall, T. Takenaka, and M. Tanaka, "Conjugate gradient method applied to inverse scattering problems," *IEEE Trans. Antennas Propag.*, vol. 43, no. 8, pp. 784–792, Aug. 1995.
[18] T. K. Sarkar and S. M. Rao, "The application of the conjugate gradient method for the solution of electromagnetic scattering from arbitrarily oriented antennas," *IEEE Trans. Antennas Propag.*, vol. AP-32, no. 4, pp. 389–403, Apr. 1984.
[19] R. Devayya and D. J. Wingham, "The numerical calculation of rough surface scattering by the conjugate gradient method," *IEEE Trans. Geosci. Remote Sens.*, vol. 30, no. 3, pp. 645–648, May 1992.
[20] Z. Wu, "Tomographic imaging of isolated ground surfaces using radio ground waves and conjugate gradient methods," *Proc. Inst. Elect. Eng.—Radar Sonar Navigat.*, vol. 148, no. 1, pp. 27–34, Feb. 2001.
[21] A. Quarteroni, R. Sacco, and F. Saleri, *Numerical Mathematics*. New York, NY, USA: Springer-Verlag, 2000.
[22] H. Brezis, *Functional Analysis, Sobolev Spaces and Partial Differential Equation*. Heidelberg, The Netherlands: Springer-Verlag, 2011.
[23] F. Schopfer, A. Louis, and T. Schuster, "Nonlinear iterative methods for linear ill-posed problems in Banach spaces," *Inv. Prob.*, vol. 22, no. 1, pp. 311–329, Feb. 2006.
[24] F. Lenti, C. Estatico, S. Gratton, and D. Titley-Peloquin, "Conjugate gradient method for p-norm minimization," to be published.
[25] W. Hager and H. Zhang, "A survey of nonlinear conjugate gradient methods," *Pacific J. Optim.*, vol. 2, no. 1, pp. 35–38, 2006.
[26] F. Lenti, "Regularization methods in Hilbert and Banach spaces for remote sensing applications," Ph.D. dissertation, Dipartimento di Scienze e Alte Tecnologie, Univ. dell'Insubria, Como, Italy, Feb. 2015.
[27] S. Gratton, P. Toint, and A. Tröltsch, "An active-set trust-region method for derivative-free nonlinear bound-constrained optimization," *Optim. Methods Softw.*, vol. 26, no. 4/5, pp. 873–894, Oct. 2011.
[28] J. Hollinger, *DMSP Special Sensor Microwave/Imager User's Guide*. Washington, DC, USA: Naval Res. Lab., 1987.
[29] F. Lenti, F. Nunziata, C. Estatico, and M. Migliaccio, "Analysis of reconstructions obtained solving l^p-penalized minimization problems," *IEEE Trans. Geosci. Remote Sens.*, vol. 53, no. 9, pp. 4876–4886, Sep. 2015.

Flavia Lenti (S'11) received the B.Sc. and M.Sc. (*summa cum laude*) degrees in applied mathematics from University of Rome "La Sapienza," Rome, Italy, in 2006 and 2009, respectively, the Master's degree in space remote sensing technology from the Italian Space Agency (ASI), Rome, in 2011, and the Ph.D. degree in applied mathematics from the University of Insubria, Como, Italy, in 2015.

Since 2011, she has been cooperating with Remote Sensing Laboratory of Università degli Studi di Napoli "Parthenope," Napoli, Italy, working on resolution enhancement of radiometer data. She is currently a Researcher with Institut de Recherche en Informatique de Toulouse, École nationale supérieure d'électronique, d'électrotechnique, d'informatique, d'hydraulique et des télécommunications, Toulouse, France, and with Centre Européen de Recherche et de Formation Avancée en Calcul Scientifique, Toulouse. Her research activities deal with numerical linear algebra, inverse problems applied to remote sensing data, image restoration, and data assimilation.

Ferdinando Nunziata (S'03–M'12–SM'14) was born in Italy in 1982. He received the B.Sc. and M.Sc. (*summa cum laude*) degrees in telecommunications engineering and the Ph.D. degree (curriculum electromagnetic fields) from Università degli Studi di Napoli "Parthenope," Napoli, Italy, in 2003, 2005, and 2008, respectively.

Since 2010, he has been an Assistant Professor of electromagnetic fields with Università degli Studi di Napoli "Parthenope." Since 2013, he has been also a Guest Professor with Shanghai Ocean University, Shanghai, China. He has authored/coauthored over 45 peer-reviewed journal papers. His main research interests deal with applied electromagnetics, including electromagnetic modeling, single- and multipolarization sea surface scattering, radar polarimetry, synthetic aperture radar sea oil slick and metallic target monitoring, spatial resolution enhancement techniques, and Global Navigation Satellite System Reflectometry.

Dr. Nunziata was/is in the organizing committee of the 2008, 2010, 2012, and 2014 IEEE Graduate of Last Decade (GOLD) Remote Sensing Conferences at the European Space Agency, Frascati, Italy; at the Italian Naval Academy, Livorno, Italy; at the National Research Council, Rome, Italy; and in Berlin, Germany, respectively. He is a Young Professional (formerly GOLD) Representative to the Geoscience and Remote Sensing Society AdCom and to the IEEE Italy Section. He was the recipient of the 2003 IEEE GRS South Italy Chapter Best Remote Sensing Thesis Award, the 2009 Sebetia-Ter International Award for his research activities in remote sensing, and the 2012 Latmiral Prize, provided by the Italian Society of Electromagnetics (SIEm).

Claudio Estatico received the "Laurea" degree in mathematics from the University of Genoa, Genoa, Italy, in 1995 and the Ph.D. degree in computational mathematics and operations research from the University of Milan, Milan, Italy, in 2002.

In 2003, he was a core participant of the special semester program on inverse problems at the Institute for Pure and Applied Mathematics, University of California, Los Angeles, CA, USA. He is currently an Associate Professor of numerical analysis with the Department of Mathematics, University of Genoa. His research interests include numerical linear algebra and inverse problems: iterative regularization methods in Hilbert and Banach spaces, structured matrices and related preconditioners for linear and nonlinear ill-posed problems, inverse scattering, and remote sensing.

Maurizio Migliaccio (M'91–SM'00) received the Laurea degree (*summa cum laude*) in electronic engineering from the Uni-versità degli Studi di Napoli Federico II, Napoli, in 1987.

Since 2005, he has been a Full Professor of electromagnetics with Università degli Studi di Napoli "Parthenope," Napoli, Italy, where he is also the Chairman of the telecommunication courses. Since 2013, he has been also an Affiliated Full Professor with Nova Southeastern University, Fort Lauderdale, FL, USA. He has been teaching microwave remote sensing since 1994. He has been a Member of the Italian Space Agency (ASI) scientific committee, an ASI delegate at e-geos AdCom, and a Member of ASI CSG panel. He has been a member of ESA PB-EO. He has been a Visiting Scientist with Deutsche Forschungsanstalt fur Lüft und Raumfahrt (DLR), Oberpfaffenhofen, Germany. He has lectured in Italy, USA, Germany, Spain, Czech Republic, and China. He is the Italian delegate at EU COST SMOS Mode Action. He authored or coauthored over 100 peer-reviewed journal papers on remote sensing and applied electromagnetics. His current scientific interests cover synthetic aperture radar oil slick and man-made target monitoring, remote sensing for marine and coastal applications, polarimetry, inverse problem for resolution enhancement, and reverberating chambers.

Prof. Migliaccio has been a promoter and organizer of the IEEE GOLD Remote Sensing Conferences and a Chairman of the IEEE GRS South Italy Chapter. He is an Editor of the International Journal of Remote Sensing Associate and an Associate Editor of the special issue on CosmoSkyMed of IEEE JOURNAL OF SELECTED TOPICS IN APPLIED EARTH OBSERVATIONS AND REMOTE SENSING.